



Stretchable graphene and carbon nanofiber capacitive touch sensors for robotic skin applications



Srinivasarao Yaragalla ^{a,*}, Simeone Dussoni ^{b,*}, Muhammad Zahid ^a, Marco Maggiali ^b, Giorgio Metta ^b, Athanassia Athanasiou ^{a,*}, Ilker S. Bayer ^{a,*}

^a Smart Materials, Istituto Italiano di Tecnologia, Via Morego 30, Genova 16163, Italy

^b iCub Facility, Istituto Italiano di Tecnologia, Via Morego 30, Genova 16163, Italy

ARTICLE INFO

Article history:

Received 12 January 2021

Revised 15 May 2021

Accepted 29 May 2021

Available online 7 June 2021

Keywords:

Graphene

Carbon nanofiber

Electrical properties

Nanocomposites

Morphology

Touch sensor

ABSTRACT

Stretchable capacitive tactile sensors are crucial for the current and future soft robotic technology, particularly for designing artificial electronic skin for robots. In this study, we fabricated stretchable electronic tactile sensors by spray coating of conductive graphene nanoplatelets (GNPs) or carbon nanofibers (CNFs) with liquid natural rubber (NR) binder over stretchable nitrile rubber (NBR) sheets. CNF-based coatings showed remarkably low sheet resistance of $30 \Omega \text{ sq}^{-1}$ and much better current transmission patterns under elongation, with ~50% current transmission reduction under 50% elongation, compared to GNP-based coatings with $600 \Omega \text{ sq}^{-1}$ resistance and ~99% current transmission reduction under 50% elongation. Structural damages/cracks within the coatings due to repeated stretch-release cycles could be healed by a rapid convective heat annealing process, restoring to initial current. Haptic sensing properties of the fabricated flexible capacitive device based on CNFs-coated nitrile rubber were evaluated by connecting it to a printed circuit board (PCB). The device could easily sense tactile forces from tens of mN to a few N, corresponding to $(10^{-2}-10)$ kPa pressure range over curvilinear surfaces or under elongation.

© 2021 The Korean Society of Industrial and Engineering Chemistry. Published by Elsevier B.V. All rights reserved.

Introduction

Robotic material technologies have received significant attention from researchers and industrialists owing to the diversity of implications in our day-to-day life [1–4]. Smart design of flexible and mechanically robust devices for a wide range of robotic skin applications is one of the main requirements to overcome stretching induced issues and mechanical failure of integrated devices based on soft materials. Such devices that enable and improve robots' compliance are essential for robots to interact with humans and the environment, in areas such as soft robotics, prosthetics, and so on [5,6]. Inspired by the physio-mechanical construction of biological tissues and skin, and considering the human tactile mechanisms as a model, a variety of artificial skin substrates have been developed for Robotics with intelligent materials to identify various stimuli such as stretch, temperature, and mechanical pressure [7,8].

Tunable deformable capacitors can be easily stimulated by applying pressure, torsion, and shear as crucial parts of the stretchable sensors [9,10]. Many reports have been published on compliant and flexible capacitive devices dedicated to electronic skin applications for robotic technology [11–13]. It is very important for such devices to function under elongation (more than 100%) apart from being flexible [14]. In addition, desirable characteristics are a low hysteresis (especially against mild friction and touch), a low cost, and easy integration on curvilinear surfaces [15,16]. Depositing or encapsulating metal nanowires [17], carbon nanofibers (CNFs) [18,19], liquid metals [20] and other conducting fillers, as electrodes on elastomer-based matrices/polymers, like poly-dimethylsiloxane (PDMS), is the most utilized approach to fabricate stretchable capacitors but also other electronic devices [21–23]. Since carbon nanomaterials, such as carbon nanofibers, carbon nanotubes, graphene nanoplatelets (GNPs), are now produced on a large scale with moderate prices [24–26], they are becoming a more and more frequent choice as the conductive filler to embed in the elastomer/polymer matrix for stretchable capacitors and electronics in general.

* Corresponding authors.

E-mail addresses: Srinivasa.Yaragalla@iit.it (S. Yaragalla), Simeone.Dussoni@iit.it (S. Dussoni), Athanassia.Athanasiou@iit.it (A. Athanasiou), Ilker.Bayer@iit.it (I.S. Bayer).

Supercapacitors and strain sensing devices based on carbon nanotubes have been documented in the literature working under cyclic mechanical stretch [27]. CNFs have been utilized also for fabricating flexible electrochemical capacitors [28] and efficient stretchable conductors [29]. GNPs that are graphene layers stacked together, can be processed *in situ* within the polymers in such a way that under stretching, their devices can exhibit supercapacitance [30,31]. At present, there is a demand for stretchable capacitive sensors that can function at 100% or even longer elongation levels, since they are strategic for soft robotics and especially for artificial skin application. Key factors for such devices are the ease of production, scalability of devices, use of low environmental and economic impact production techniques, and biocompatible and possibly biodegradable materials.

In the present work, we report the fabrication of stretchable capacitive devices by spray coating of Nitrile Butadiene Rubber (NBR) films with suspensions of graphene or carbon nanofibers and liquid natural rubber (NR) in methyl isobutyl ketone solvent. The fabrication method can be easily scaled up and is commercially viable. A big challenge of the developed devices is the adhesion of the conductive ink (graphene or CNFs) on the surface of the NBR, as it should be stretched while functioning as a tactile sensor. The liquid natural rubber apart from functioning as the binder of the conductive coating also demonstrated strong substrate adhesion under tension. The performance of the developed capacitive sensor was tested under various conditions, particularly applying different loads (from 125 g to 1875 g) and showed significant capacitance variation in the range of 1–10 pF.

Materials and methods

As stretchable substrates were used areas of nitrile rubber (acrylonitrile butadiene) gloves, obtained from NaturSint. GNPs (grade ultra G+) were obtained by Directa Plus S.p.A (Italy). Graphitized CNFs (diameter \approx 100 nm, length from 20 to 200 μm) were purchased from Sigma-Aldrich (grade PR-25-XT-HHT from Pyrograf Products Inc.). The detailed morphology and characteristic properties of GNPs and CNFs materials utilized in this work were studied earlier by our group and will not be repeated herein for brevity [29,32]. Liquid, uncross-linked natural rubber (NR) dispersion (FixoGum, 33 wt% in heptane) was obtained from Marabu GmbH&Co.KG, Germany, and 4-methyl 2-pentanone solvent was received from Sigma Aldrich, Italy. All polymers and solvents were used as received.

Preparation of NR polymer-CNF/GNP suspension inks and coating process

Typically, the conductive polymeric slurry was prepared by mixing 3.63 g of liquid NR polymer, which contains 1.2 g of dry NR (33 wt.% rubber in heptane) and 0.36 g of CNFs or GNPs (30 wt% relative to dry NR weight). Specifically, 0.36 g of CNFs/GNPs and 3.63 g of liquid NR gum were put into a beaker, where 60 ml of 4-methyl 2-pentanone solvent were added. Thereafter, the resulting suspension was mechanically agitated for 2 h using an agitator. Then, the obtained conductive slurry was tip sonicated (20 kHz, 750 W, 40% amplitude, 2 times for 25 sec) using a Sonics & Materials, Inc. sonicator (Model Num. VCX750) to obtain a homogeneous dispersion. Before coating, to improve their surface adhesion, the NBR substrates were immersed in 50% acetic acid aqueous solution for 1 $\frac{1}{2}$ hours and dried. Surfaces of 9.9 cm^2 of the NBR substrates were spray-coated using a total of 30 ml of the dispersion, in 5 ml steps due to spray gun reservoir size of the Paasche Airbrush (U.S.A.). Around 15 cm distance from Airbrush to nitrile sheet and 2.0 bar pressure were maintained during

spray coating. Heat gun treatment (\sim 140–150 °C, 16–17 cm distance, 60 sec) was employed after spraying to speed up the solvent's evaporation and improve adhesion.

Scanning electron microscopy and fourier transform Infrared, FTIR, spectroscopy

The cross section and the surface morphology of the prepared samples were investigated with a JEOL microscope (model JSM-6490LA, acceleration voltage of 10 kV). The specimens were frozen in liquid nitrogen and fractured by tweezers prior to take cross sectional images. FTIR spectra of the prepared composites were recorded with a Bruker Vertex 70v wavenumber ranging from 1000 to 4000 cm^{-1} with the resolution of 2 cm^{-1} and averaging 128 scans.

Current-voltage measurements

The effect of cyclic and stepwise deformation on the current flowing through the nanocomposite at constant voltage was investigated by four-probe Keithley 2611A source meter coupled with Deben custom-designed dual-screw uniaxial testing machine. Adhesive Cu tape electrodes were connected to the specimens ends spaced by 9 mm. Samples were stretched to $\Sigma_{50\%} = 50\%$ elongation, with 5 mm. min^{-1} elongation rate, and then were released to a deformation of 20% of the initial length $\Sigma_{20\%}$.

Tensile measurements

Tensile characteristics of the prepared films were investigated with an Instron dual column table top universal testing system 3365 (USA) at 10 mm min^{-1} strain rate. Measurements were conducted on five different specimens for each sample.

Capacitance measurements

In a tactile capacitive transducer a deformable dielectric is pressed by the applied force and the corresponding capacitance variation is measured and can be converted back to the force value. We recorded the capacitance values or signals from the stretchable capacitors with a commercial Capacitance-to Digital Converter (CDC, the AD7147 from Analog Devices [33]): this device is robust and used extensively in capacitive touch devices. It features a sensitivity of 13 fF/LSB and adjustable offset, with a 16 bits dynamic range. For our purposes, we limited the dynamic range to 8 bits, which is sufficient to encode the range of forces in artificial skins. The device has an I2C interface readout through a dedicated Microcontroller Tactile Board (MTB) developed at IIT for the iCub robot [34].

Results and discussion

Conductive ink coated flexible elastomer film morphology

In general, incorporation of GNPs or CNFs into nitrile rubber (NBR) to produce a conductive composite is made by the rubber vulcanization process [35]. Herein, instead, conductive coatings based on GNPs or CNFs with natural rubber as binder were applied over NBR by spray coating. Scanning electron microscopy images of GNPs or CNFs-coated nitrile rubber films are illustrated in Fig. 1(a–h), showing coating cross-sections and surface morphology. The sprayed nanocomposites formed homogeneous coatings over the NBR surface. The cross-section images of rubber films with GNPs/CNFs coating are summarized in Fig. 1 (a) & (e). The coating thickness of both GNPs and CNFs was around \sim 30 \pm 5 μm . The conduc-

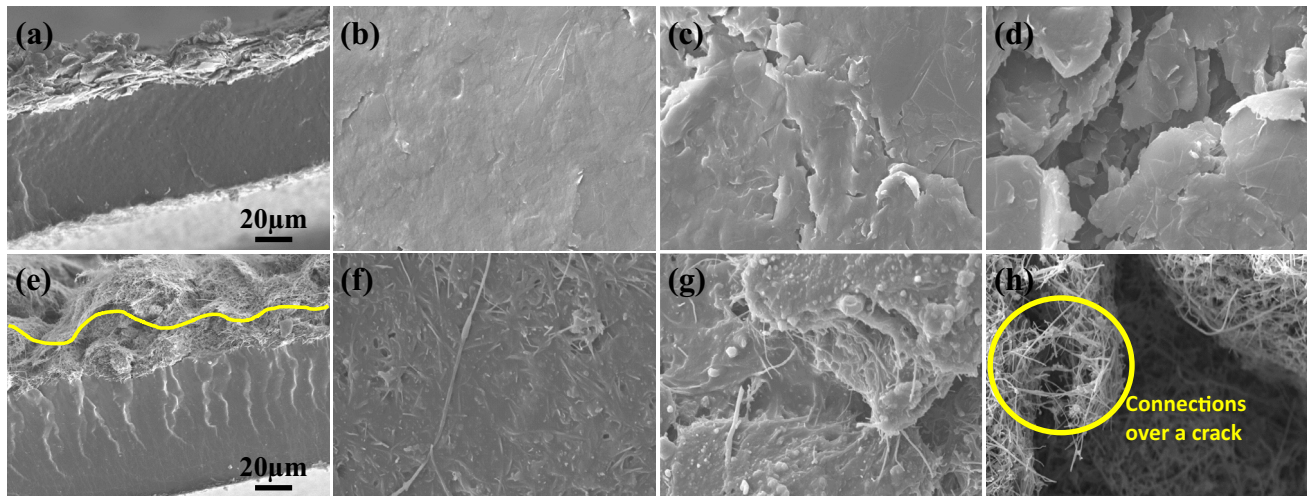


Fig. 1. (a) SEM cross section & (b) surface morphology of GNP-coated NBR before elongation; surface morphology of GNP, (c) after cyclic (stretched up to 50% and releasing back to 20% of initial length) & (d) sequential elongation (elongation of 5% steps up until 50%); (e) cross section (indicated with yellow dots) & (f) surface morphology of CNF-coated NBR before elongation; surface morphology of CNF (g) after cyclic & (h) sequential elongation. (For interpretation of the references to colour in this figure legend, the reader is referred to the web version of this article.)

tive coatings seems appear to be well adhered to the NBR surface, as seen in the SEM images Fig. 1 (a) & (e).

NBR surfaces previously cleaned/etched by acetic acid immersion treatment had surface features (See [supporting information Fig. S1](#) (a) & (b)) that enabled adhesion of the conductive coatings. The pristine nitrile rubber thickness was measured to be ~67 μm, and it increases to ~77 μm after the treatment with 50% acetic acid, due to its partial penetration inside the rubber causing permanent partial polymer swelling (See [supporting information Fig. S1](#) (c) & (d)). FTIR measurements indicated that the acid immersion process did not alter NBR's core chemical structure (see [Fig. S2, supporting information](#)). GNPs and CNFs coatings' surface morphology was found to be similar to the nano-carbon loaded (GNPs, CNFs/CNTs) rubber composites prepared by vulcanization [36,37]. Since the main binder used in the conductive ink was liquid natural rubber (NR), rubber-rubber chemical affinity enabled the sprayed coatings to be more stable and conformable under elongation. As shown in Fig. 1 (c) & (g) for both GNPs and CNFs coatings, mild cracks form upon stretching of 50%, which are partially recovered when the sample is released back to 20% of its initial elongation. Moreover, for the CNF nanocomposite coatings where the connectivity among CNF fibers is more easily attained after cyclic stretching (stretched up to 50% and releasing back to 20% of initial length up to 50 cycles) due to their high aspect ratio (length 20–200 μm), CNFs could still remain connected within the cracks as seen in Fig. 1 (h). In fact, this crack forms after sequential elongation experiments (elongation of 5% steps up until 50%) in comparison to the crack within the GNP coatings (Fig. 1(d)).

Mechanical behavior

Stress-strain data of the untreated, 50% acid-treated, GNPs, and CNFs coated NBR films are summarized in [Table 1](#). The untreated

nitrile rubber showed an elastic modulus of 4.5 ± 0.6 MPa, (@ 40% strain) which is a typical value for elastomeric materials [38], and it exhibited elongation at break of 785 ± 83 % (see [supporting information Fig. S3](#)). Upon acid solution immersion, ~3 times decrease in elastic modulus (1.4 ± 0.5 MPa) was noticed for NBR films while they displayed a small increase in elongation at break (900 ± 55 %). The attributing factor for this behavior is that the acetic acid molecules may disrupt the crosslinks of NBR, and act as a plasticizing agent increasing polymeric chain mobility [39]. In the case of NBR films coated with 30 wt% GNPs coating, the bilayer displayed increased elastic modulus, by ~2.9 and ~9.3 times compared to the untreated and acid-treated NBR, respectively. The reason for such an improvement in modulus is due to the dispersion of GNPs within NR polymer and is associated with the intrinsic property of graphene. There is a sudden drop in stress after around 40–50% strain, which is also well corroborated with an electrical performance in which 99% current drop is noticed at 50% stretch (see [Fig. 2 \(a\)](#)). GNP-based coatings did not significantly alter the elongation at break value of the acid-treated NBR substrate as seen in [Table 1](#). In contrast, CNFs based coatings did not significantly alter the elastic/Young's modulus of the acid-treated NBR substrates within experimental measurement error. The same effect was also noticed on the elongation at break in comparison to acid-treated NBR substrates. Considering the experimental measurement statistics listed in [Table 1](#), it may be concluded that both GNP and CNF based coatings show a conformal mode of adhesion to the substrates (acid modified) without any detrimental effects on the elongation characteristics of NBR (see Fig. 1 (a) & (e)).

Electrical performance under elongation

[Figs. 2 & 3](#) demonstrate the electric current response of 30 wt.% GNPs and CNFs-based coatings under 2 V constant bias, upon stretch-release cycles shown schematically in [Fig. 2\(a\)](#) and the photographic images are illustrated in [Fig. S4](#) (see [Supporting Information](#)). The current is normalized by its initial value and reported as I/I_0 . Each coated sample was elongated up to 50% (step A) and allowed to relax back to 20% elongation (step B), and this cycle was repeated 50 consecutive times. We choose the 50–20% stretch-release cycle, considering that human joints (fingers, knees, and elbows) experience a similar range of strain during

Table 1
Stress-strain data of NBR composites.

Sample	Modulus (MPa)	Elongation (%)
Untreated NBR	4.5 ± 0.6	785 ± 83
Acid-treated NBR	1.4 ± 0.5	900 ± 55
GNP30% on acid-treated NBR	13.0 ± 0.7	861 ± 75
CNF30% on acid-treated NBR	2.0 ± 0.5	820 ± 70

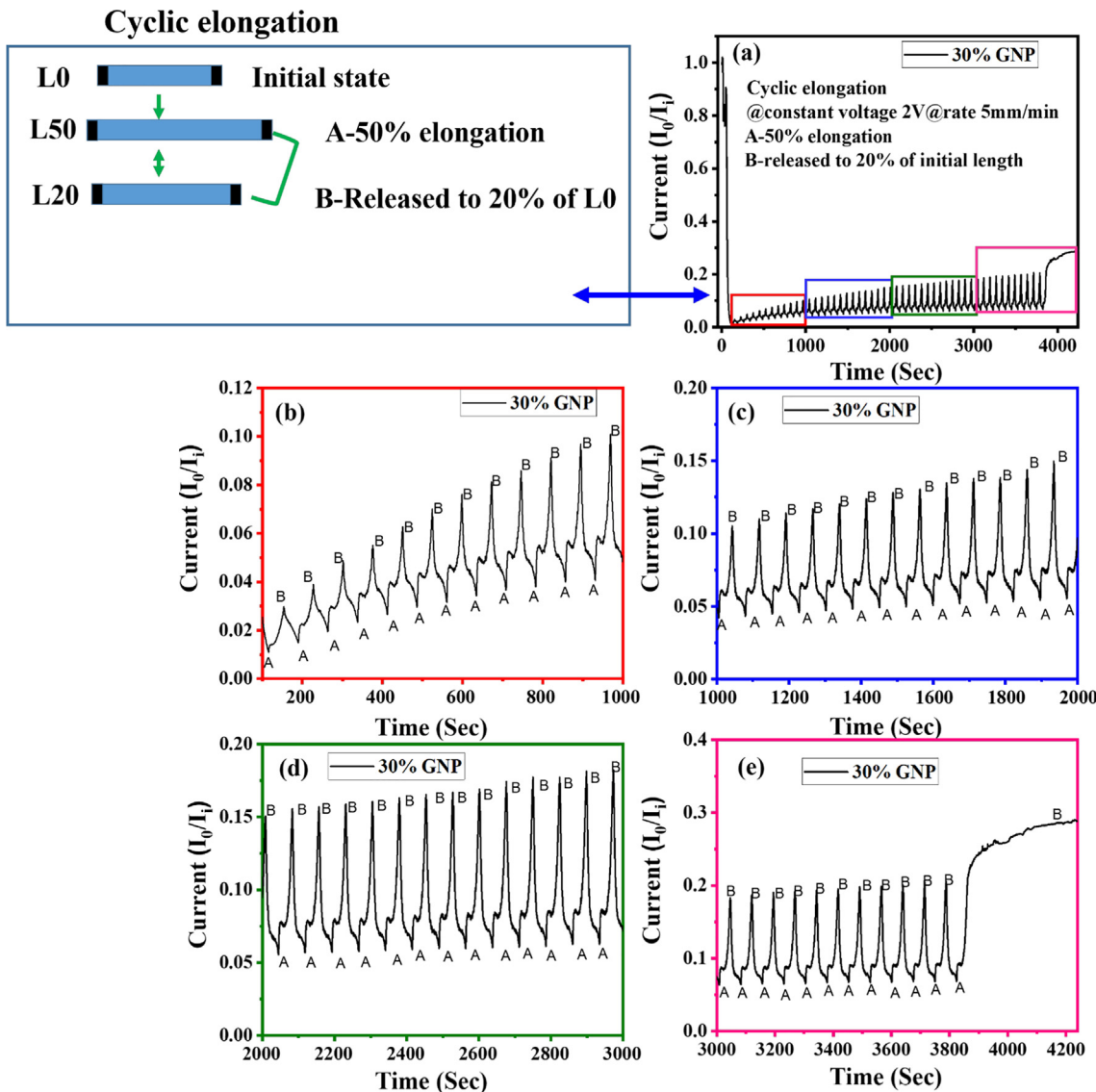


Fig. 2. Electrical characteristics of the 30 wt.% GNP (a) (b) (c) (d) (e) @50% elongation (step A) and released to 20% (step B) of initial length.

motion [40]. The measured current is thus related to conductivity change in a realistic scenario, which is important to ensure proper working of the tactile sensing device and its interconnections.

Upon first stretching, GNP-based coatings showed a far greater decrease in the current (electric current dropped by 99%, i.e., $I_0/I_i = 0.01$) (see Fig. 2(a)) corresponding to a change of conductivity of about two orders of magnitude. Instead, CNF-based coatings showed lower drop in current by about 46% (i.e., $I_0/I_i = 0.54$) (see Fig. 3(g)). Upon successive stretch-release cycles, the current seems to partially recover towards the initial value.

In particular, in the case of GNP coatings, the highlighted regions in Fig. 2(a) are expanded in Fig. 2(b), (c), (d) & (e) showing a small shoulder or hump during release (step B), which becomes more significant as the number of stretch-release cycles increases. The rationale for observing such a hump may be associated with relaxation of NBR rubber and stereoregularity of natural rubber chains (cis-1, 3-poly isoprene), which is the matrix of the conductive coating [41]. The current recovery increases gradually with the increment of stretch-release cycles and at some point it reaches a saturation point (i.e., from $I_0/I_i = 0.01$ to $I_0/I_i = 0.28$) (see Fig. 2(e)). It is worth mentioning that the current recovery in step B is higher than in step A.

Stretch-release cycles of CNFs based coatings (highlighted regions with red, blue, green, and pink colors) are illustrated in Fig. 3 (g), (h), (l), (j) & (k). The current recovery (step B) reached a stable value from $I_0/I_i = 0.54$ to $I_0/I_i = 0.73$ (see Fig. 3 (k)) much quicker than the GNP system. The current of the CNF-based coatings was affected less upon elongation most likely due to the density of contacts established between long carbon fibers (see SEM image in Fig. 1(h)).

Although overall electrical current loss in GNP coatings is much higher upon elongation than in the CNF-based coatings, they feature better current recovery (i.e., from $I_0/I_i = 0.01$ to $I_0/I_i = 0.28$, see Fig. 2(e)) compared to CNF coatings (i.e., from $I_0/I_i = 0.54$ to $I_0/I_i = 0.73$, see Fig. 3(k)). This can be attributed to their ability to reorganize themselves inside the matrix upon release [42]. On the contrary, the partially orientated carbon nanofibers upon elongation are expected to have difficulty in restoring their original random morphology. Interestingly, we found that stretch-induced cracks (Fig. 1 (c) & (g)) inside the coatings can be healed by annealing with a simple heat gun procedure, which is identical to the fabrication process (see section 2.1). After a simple convective annealing step, both GNPs and CNFs based coatings fully recover their initial current (see Fig. 4 (a) & (b)). Disappearance of

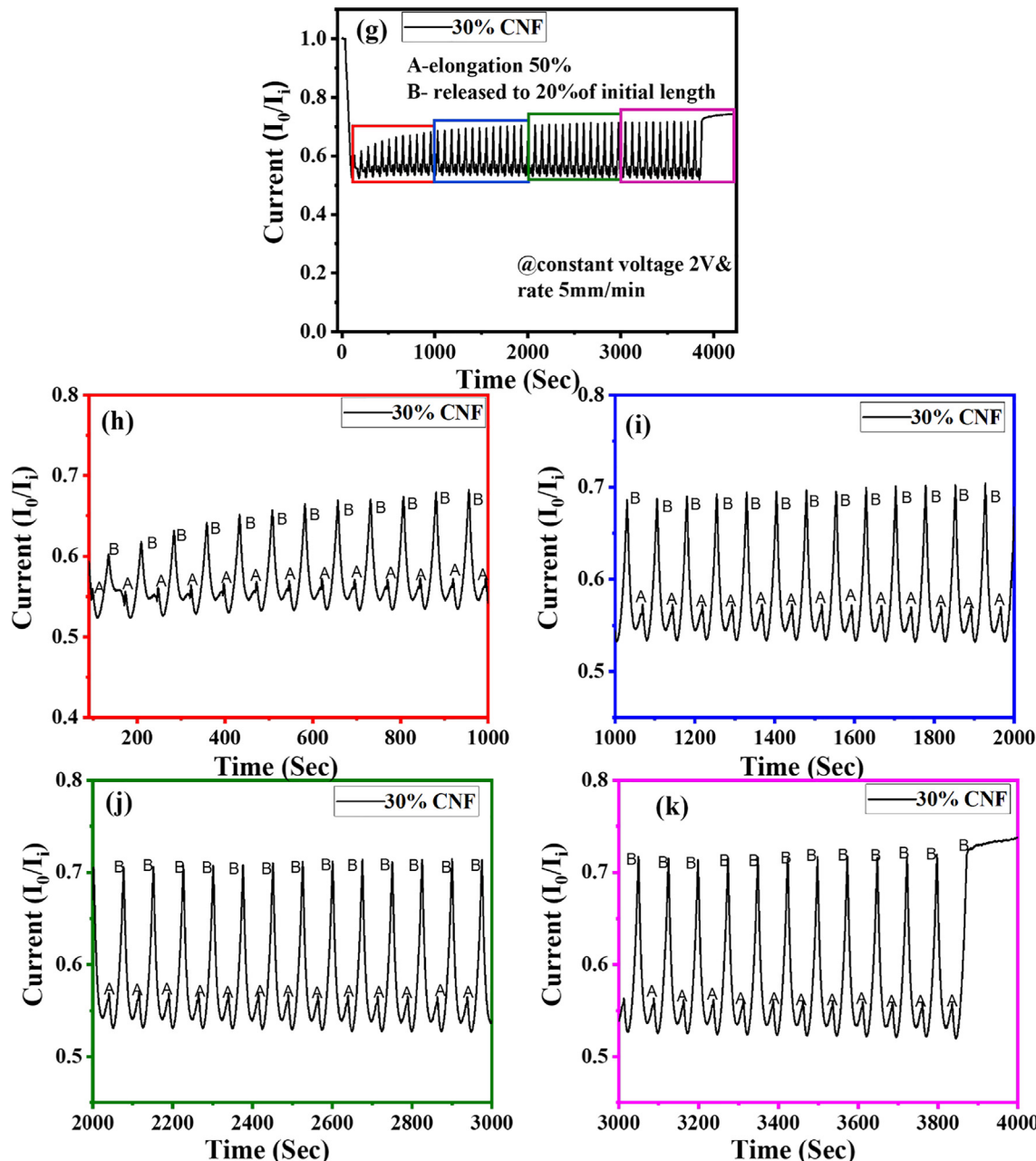


Fig. 3. Electrical characteristics of the 30wt% CNF (g) (h) (i) (j) (k) coated nanocomposites @50% elongation (step A) and released to 20% (step B) of initial length.

the mild cracks after the annealing process was also confirmed by electron microscopy inspection (see [supporting information Fig. S5 \(b\) & \(d\)](#)). The plausible reason for healing mild cracks is that we used liquid uncrosslinked NR as one of the main ingredients in the conductive ink and we annealed the samples at ~ 150 °C, the rubber becomes soft and fused at that temperature with the capability to heal structural damages. We observed 30% CNFs-based coatings have a uniform current response within the experiment time (100Sec) after the cyclic test due to the network formation (structural restoration) of long CNFs (length 20–200 μm) after the cyclic stretch (see SEM image [Fig. S5 \(d\)](#) in [supporting information](#)).

The electric current was also measured under sequential elongation for coatings with 30 wt% GNP and CNF concentrations, as shown in [Fig. 4\(c\)](#). Each sample was elongated with 5% steps up to 50% (L0-L50). A short time gap (~ 50 s) was allowed for measur-

ing the current at each increment step under a constant bias of 2.0 V. GNPs based coatings exhibited 52% drop of the initial current at 5% elongation, and about 99% of the initial current is lost at 50% elongation. In contrast, CNFs based coatings showed 10% and 50% drop in the initial current at 5% and 50% elongations, respectively (see [Fig. 4\(c\)](#)). One of the attributing factors for current drop difference is the aspect ratio of the two conductive nanomaterials. The length of the CNFs ranges from 20 to 200 μm , whereas the GNP lateral size ranges from hundreds of nanometers to few micrometers [29,43]. Thus, CNFs may still remain connected within elongation-induced cracks and tend to align parallel to the stress direction [44]. On the other hand, the GNPs can disconnect during elongations causing a more prominent drop in the current. The difference in the current drop upon elongation of the two types of coatings clearly substantiated earlier experimental observations in which almost similar reduction in current (99% for GNP&~50% for CNF

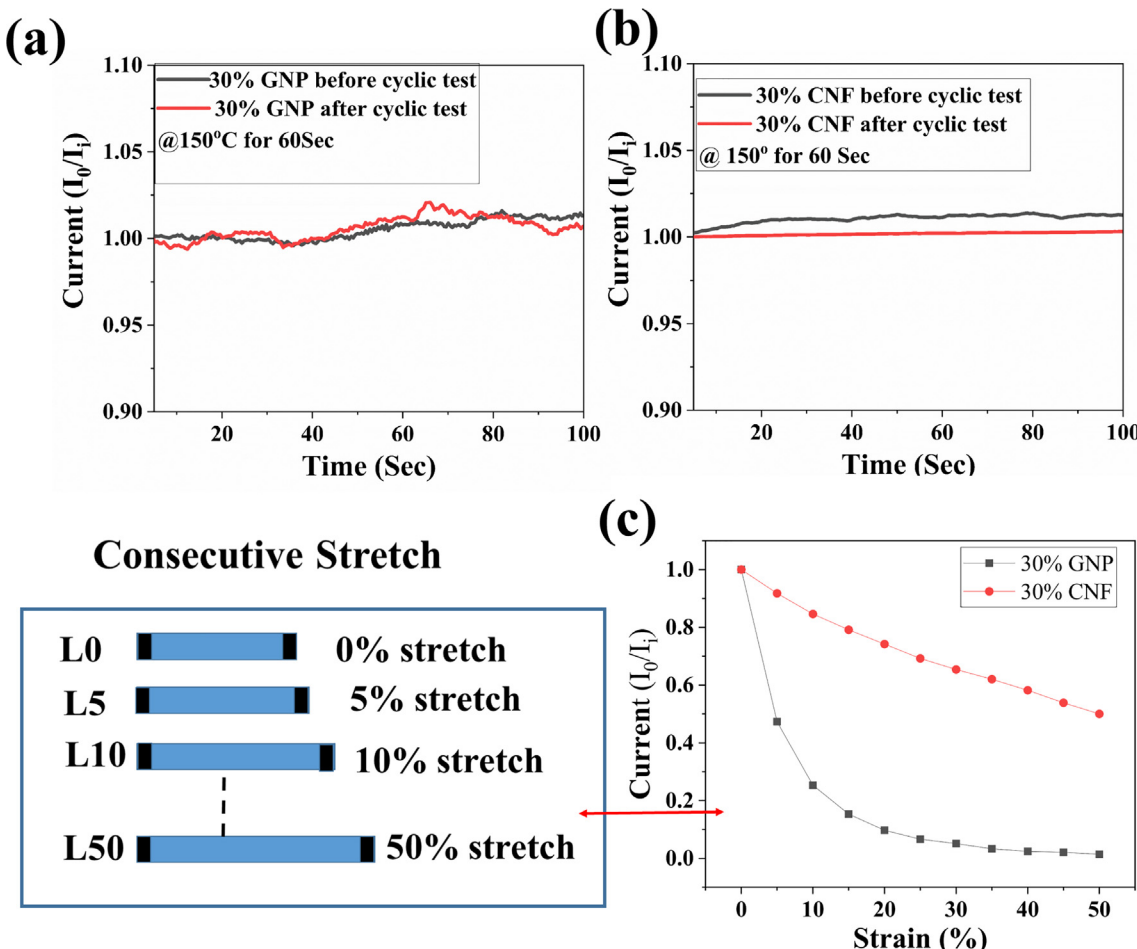


Fig. 4. Current recovery of GNP (a) and CNF (b) based coatings after convective annealing with a heat gun; electrical current response of the GNP and CNF based coatings with respect to consecutive stretch (c).

upon 50% stretch) was recorded for both GNP and CNF based coatings. By conducting the electrical current experiments before fabricating the stretchable tactile sensors, we ensured that the current variations measured under repeated strain were within the operational response range of typical stretchable parallel plate capacitors designed to detect tactile stimuli (particularly CNF based coatings) [11,45].

To resemble a robotic motion, additionally, we first applied to the samples 10 consecutive stretch-release cycles, then we waited for stabilization of the current, and finally we stretched the samples to 50% and released them to 20% of elongation (see Figs. 5 & 6). The aforementioned 99% and 50% initial current drop values were measured for GNP and CNF based coatings, respectively, upon 50% elongation, also in this case. After the first 10 cycles, and the subsequent application of 50% stretching, the current dropped from $I_0/I_i = 0.2$ to $I_0/I_i = 0.04$ (see Fig. 5) for GNP coatings, while for the CNF coatings the drop was from $I_0/I_i = 0.66$ to $I_0/I_i = 0.5$ (see Fig. 6). At the end of the experiment, GNP-based coatings showed better current recovery (i.e., from $I_0/I_i = 0.01$ to $I_0/I_i = 0.19$) (see Fig. 5) upon relaxation compared to CNF coatings (i.e., from $I_0/I_i = 0.5$ to $I_0/I_i = 0.66$) (see Fig. 6 as discussed earlier in case of Figs. 2 & 3). Finally, all the coatings demonstrated ohmic current-voltage behavior even after elongation tests (see Figs. S6.1 & S6.2, supporting information). CNF-based coatings showed promising current values ~15.5 mA before stretching and ~8.7 mA after stretching to 50% (see Fig. S6.2 in supporting information) since they possess a high aspect ratio ((length 20–

200 μm) and could easily maintain the interconnections among them to maintain high current values. The sheet resistance of freshly made GNPs and CNFs-based coatings was $600\Omega \text{ sq}^{-1}$, and $30\Omega \text{ sq}^{-1}$, respectively (see supporting information Fig. S7). We focused on CNF-based ink devices for developing capacitive sensors based on the electrical current measurements because of their superior current performance (refer to section 3.3).

Capacitive touch sensing with stretchable electronics

Using the developed NR/CNF inks, we prepared patterned arrays of capacitive pads to measure the tactile response: we implemented an array of capacitive pads, commonly named taxels (Fig. 7(a)) [11,46]. We designed and produced a device with an equivalent taxel layout by using conventional copper technology on stretchable TPU substrates (Fig. 7(b)) [47] as a benchmark device to compare with the performance of our system. We found that the conventional TPU device maintains electrical connectivity up to only 4% stretch, which is too small for the purpose of our applications. We patterned the CNF-based device by placing a shadow mask in close contact with an NBR sheet: by spraying the CNF-NR suspension over this mask the corresponding pattern is transferred to the NBR rubber and can be characterized. Instead, the conventional device was based on a patterned horseshoe-like structure allowing the copper to follow the substrate stretching without creating internal stresses. In order to use them as tactile sensing devices, we had to match them with a deformable layer

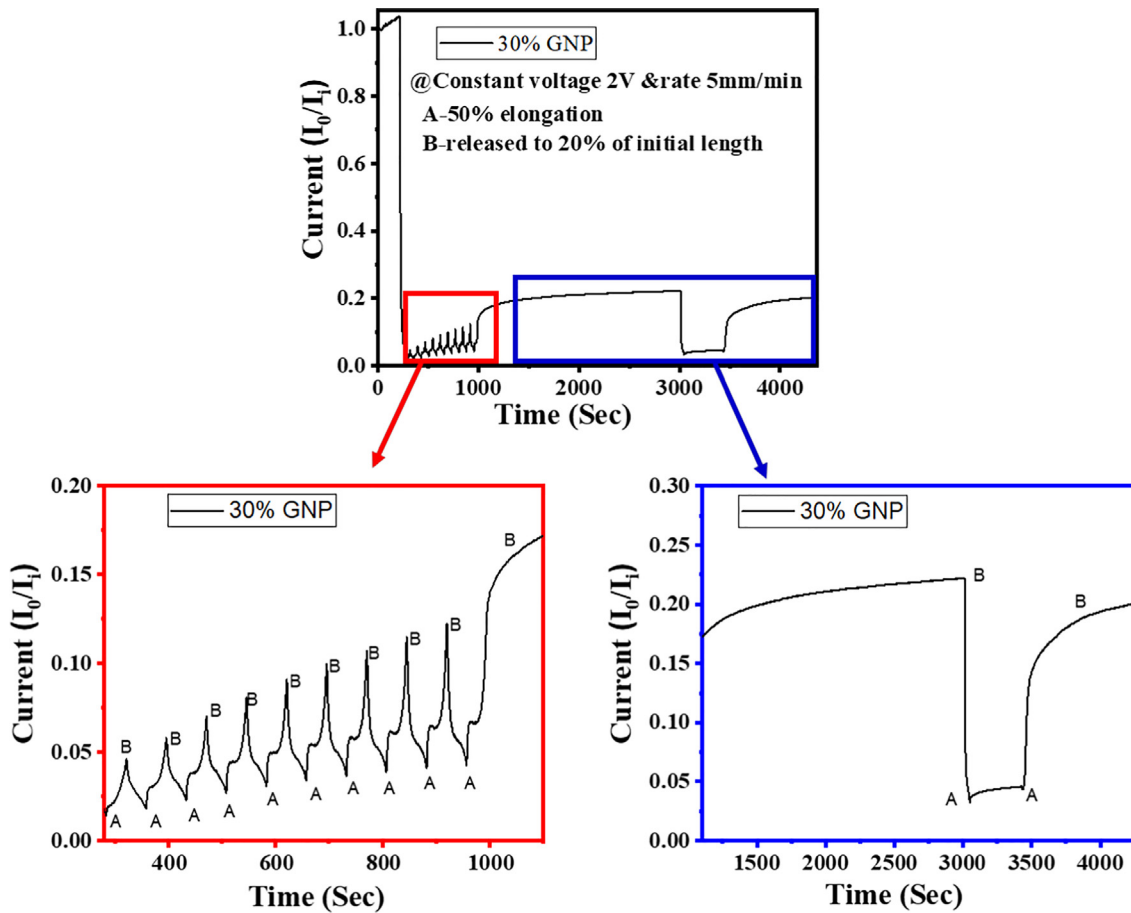


Fig. 5. Electrical current response of the GNP based coating with respect to time @50% elongation (step A) and released to 20% (step B) of initial length.

and a top electrode as schematized in Fig. 8. We chose to use a 3D mesh coupled with conductive Lycra as in iCub skin [45] to have a feeling on possible applications of the devices on robotics sensors. The deformable layer (insulator) plus the top electrode (connected to ground) provided the transduction of applied pressure or forces into electrical signals by means of a sizeable capacitance variation. In order to make sure that the signals are well-read with good noise rejection, the traces connecting the pads should be of suitable resistance. We measured resistivity on a number of locations along the CNF sprayed traces and recorded values in the range of $10\text{--}100 \Omega \text{ sq}^{-1}$ that are deemed acceptable and similar to the values presented above for the non-patterned CNF-based coating (see section 3.3). Such values also allowed us to have reliable electrical connections up to a length scale of 10 cm and even more. Here, we tested up to 10 cm due to the size of NBR films cut out of commercial gloves.

We connected the AD7147 board to the stretchable nitrile circuit by means of spring-loaded pogo-pins pressing onto the traces, as shown in Fig. 7(c). The device was covered with a piece of nylon deformable mesh, and the capacitor was realized with the top conducting layer of Lycra (see Fig. 8). We connected the Microcontroller Tactile Board (MTB) to a PC for data logging in our setup by using a commercial CAN-USB interface CANUSB-2 from ESD electronics [48]. A set of configuration commands allowed the user to set an adjustable offset. The bit-shift applied to excerpt the 8-bit packet matching the force-induced signal from the full 16-bit data word: the MTB performs this operation employing proprietary firmware. A set of measurements were taken by placing a small weight in the range 125–1875 g on top of the “skin” and recording the corresponding capacitance signals.

The proportionality of the pressure to capacitance conversion relies on the elastic properties of the nylon mesh, which has been chosen based on the experience of the iCub skin [45]. To demonstrate the feasibility of the stretchable device, we acquired the signals from the CNF-based coating in order to make sure the electrical connections are reliable: in principle we had to face both the effect of intrinsic trace resistance and the spring-loaded interface with the electronic board. As stated above we compared the signals of our device with a reference device: we designed a stretchable circuit board (SCB) based on conventional copper technology that was also covered with the same “skin” in order to have equivalent setups for both devices. The two devices were tested with the same electronics and under the same load conditions in order to have comparable results. Datagrams from the samples are plotted in Fig. 9, showing that the CNF-based devices display smooth signals with lower noise levels. This may be attributed in part due to the length of traces that is 30 cm for the copper-on-TPU device, compared to the ~10 cm of the CNF-on-nitrile.

We applied increasing loads from 1.23 N to 18.4 N in order to explore the range of response of the device. The footprint of the applied load is a circle with a diameter 45 mm; thus, the corresponding pressures lie in the range 0.7–12 kPa, which is a reasonable value for robotic grasping experiments [45]. We applied a series of weights in an increasing order from 125 g, 375 g, 875 g, 1875 g, and then the same set in decreasing order to achieve the quoted forces. Each taxel was subjected to a force proportional to its area as given by equation (1):

$$F_i = \frac{S_i mg}{\pi r^2} \alpha_i \quad (1)$$

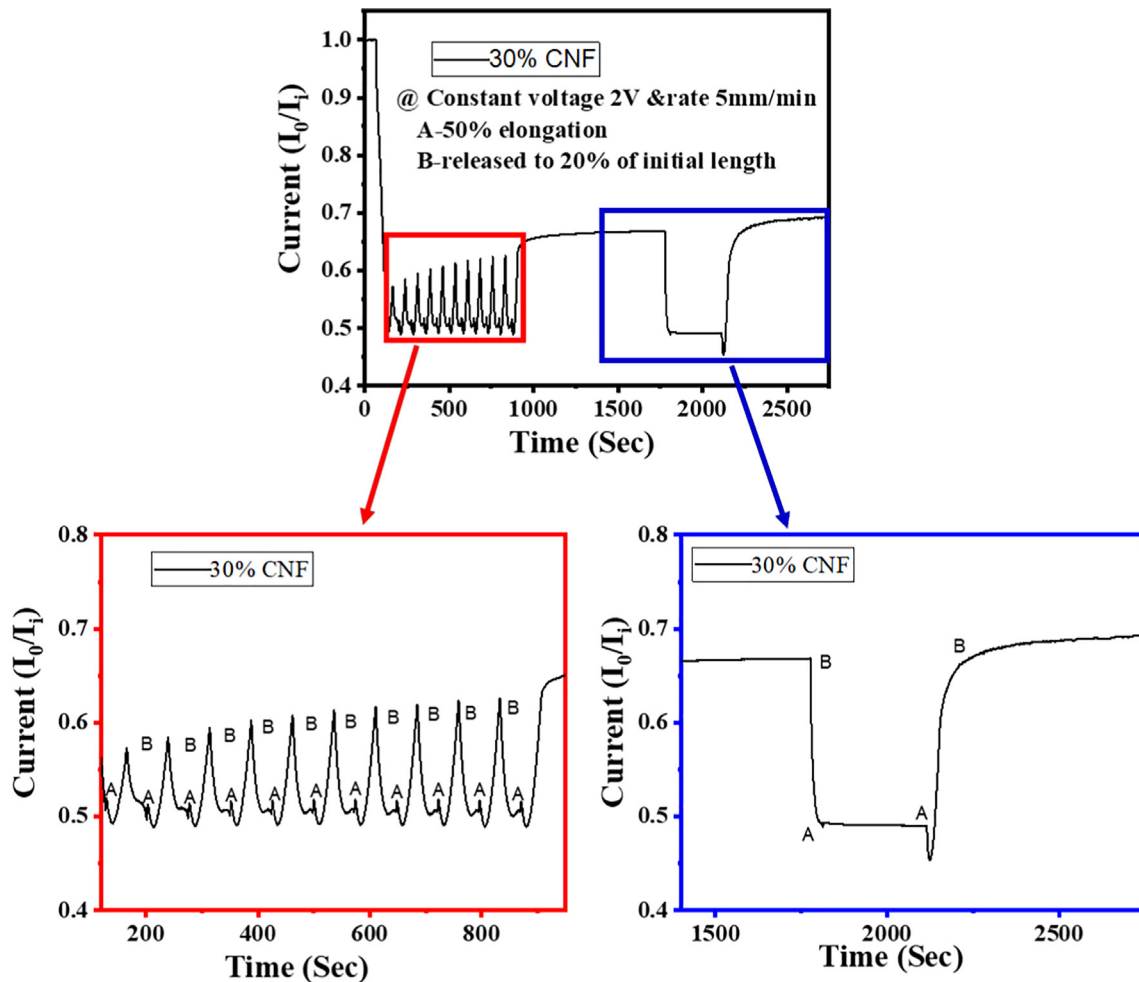


Fig. 6. Electrical current response of the CNF based coatings with respect to time @50% elongation (step A) and released to 20% (step B) of initial length.

where S_i represents i^{th} taxel area and F_i is the amount of force that is pushing on each taxel, which relates to a change in capacitance as:

$$\Delta C_i = \frac{S_i}{4\pi\epsilon_0\epsilon_r} \times \frac{F_i}{(kd - F_i)d} \frac{S_i}{4\pi\epsilon_0\epsilon_r} \times \frac{F_i}{kd^2} \quad (2)$$

where we parameterized the stiffness k of the dielectric following Hooke's law. α_i accounts for the coverage of the i -th taxel by the load itself: in order to be independent from this effect we summed up all the signals from the different taxels and investigated the proportionality of the response for the devices under test that are shown in Fig. 9 (c). With the hypothesis of full-coverage of each taxel, smaller taxels (5 mm diameter) were subject to a force as low as 0.016 N that was still detectable by our device, while larger taxels (10 mm diameter) could sense forces as high as 1 N or more without appreciable deviation from linearity. Tens of Newton could be measured by the full array; the limit to detect higher values will be dictated by the deformability of the intermediate mesh and the gain of the CDC.

The starting capacitance offset was zeroed before loading since we were only interested in capacitance variation due to applied loads. With the used loads, we recorded capacitance variations in the range of 0.9–10 pF for both devices. Sum over all taxel ensure a coherent deal of slightly different geometries. The fitting highlights good linearity of the taxel responses in the explored range of forces. Linear fit held the following results (Eqs. (3)&(4)), showing that the linear dependence has similar coefficients for both the

devices, the one made by CNF-based coatings on NBR and the commercial device made from metal conducting patterns.

We obtained the linear fitting of the capacitance versus applied pressure response, in a linear range, as:

$$CCNF = (0.85 \pm 0.03)P + (0.03 \pm 0.21) \quad (3)$$

$$CSCB = (0.70 \pm 0.05)P + (0.13 \pm 0.30) \quad (4)$$

where C and P represent capacitance in pF and applied pressure in kPa, respectively. The linear coefficient represents the tactile sensitivity of the device since it converts an applied pressure into capacitance variation. The device response in capacitance upon applied pressure is summarized in Table 2. The commercial device's performances and the nano-ink one are comparable for what concerns the capacitance variation. Our device has a lower threshold on detectable pressure: this is due to a better signal-to-noise ratio. We evaluated the threshold on minimum detectable pressure from the RMS of the no-load signals and converted them to equivalent pressure values by multiplying by the specific device slope.

The dynamic response to the applied stimulus was quite similar as expected since it depends on the geometrical parameters (mainly, the area of each taxel) and the deformable material used to convert force into deformation and, thus, capacitance variation. The speed of response is limited, in our setup, by the capacitance-to-digital conversion that takes ~10 ms to be performed due to internal settings of the IC (mainly related to filtering of the signals). Anyway, this is related to the IC, and thus it is a common feature of

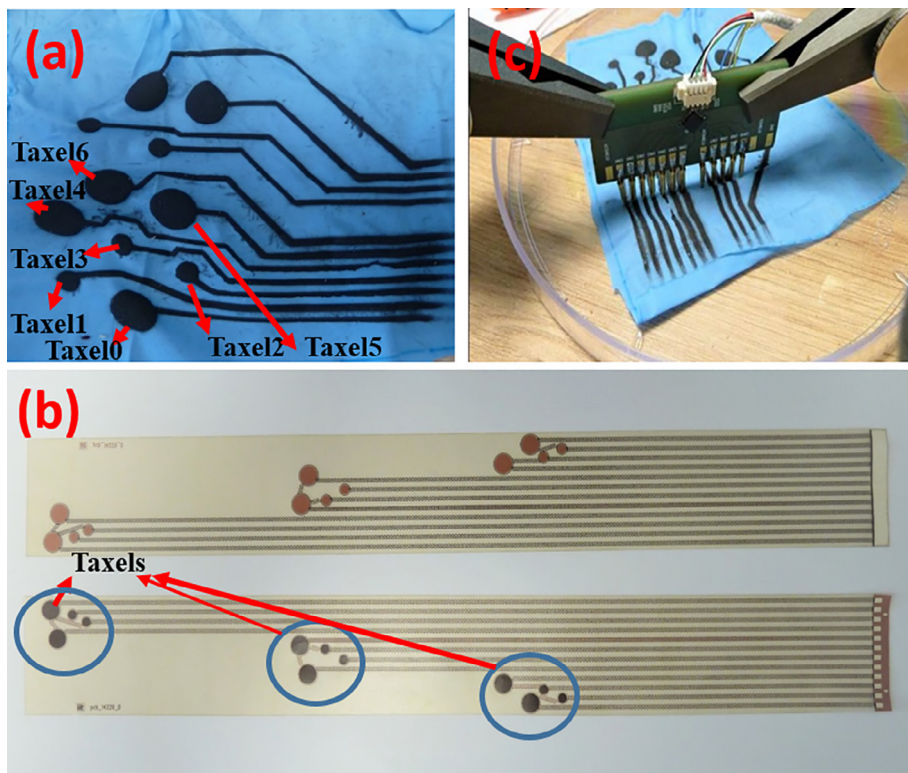


Fig. 7. The Nano-ink sprayed device on NBR sheet (a) showing the taxel arrangement and the length of patterned traces (around 10 cm), (b) the commercial TPU stretchable Circuit Board layout with the round taxels and the horseshoe structure of the interconnections. The taxels of two devices have two different sizes 5 and 10 mm diameter respectively; traces are up to 30 cm long for commercial TPU, (c) the electronic board for capacitance readout connected to the stretchable device by means of spring loaded pogo pins. The patterned structures are then covered with a deformable non-woven mesh topped with the ground electrode, to obtain the pressure sensitive capacitors, which are the basic sensing cell (taxel).

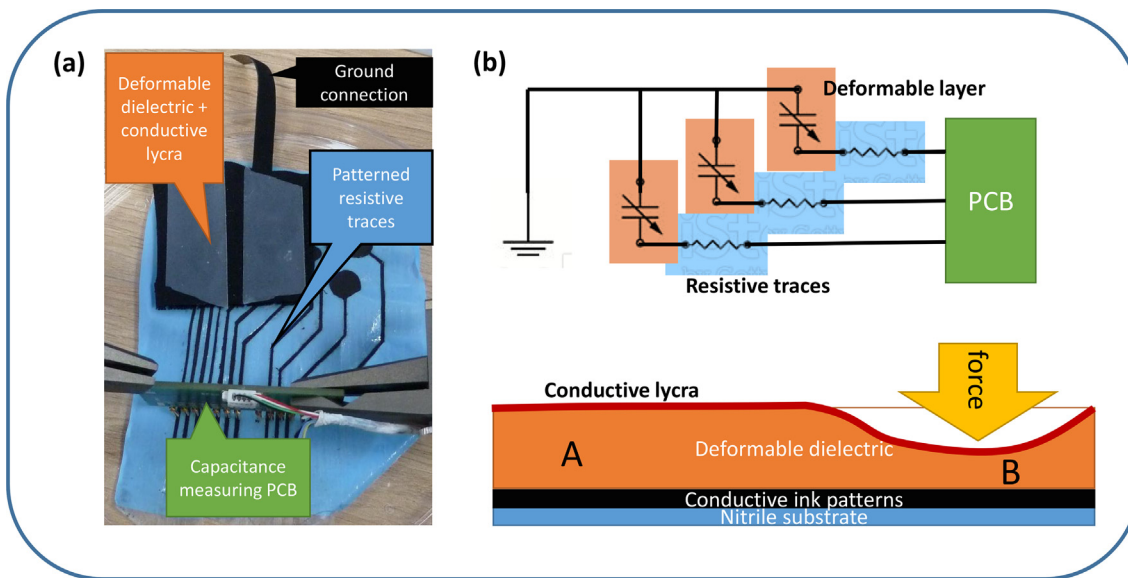


Fig. 8. (a) picture of the experimental setup with the deformable mesh + GND electrode placed on top of the stretchable device and (b) a vertical section of the setup showing the schematical representation of capacitive sensing mechanism of the tactile sensor: the unpressed mesh has a rest thickness A corresponding to a certain value of capacitance, the pressed region B has a smaller thickness: the compression is proportional to the force and the capacitance is increased correspondingly.

both setups. The leading edges of the signals are given by the speed of the pressing tool, which is in the cm/sec range. The compressed thickness is 0.5 mm thus the intrinsic stimulus is built in ~50 ms. From the signals recorded we see that a few samples are collected in the leading edge, as expected. So our electronics is well suited to

track this kind of pressure variation, i.e. equivalent to touching an object with a speed given by the joint movement. Changes in electrical currents related to applied elongation are summarized in Table ST1 (see supporting information). The conductivity drop is not affecting the capacitance measurement performed by the elec-

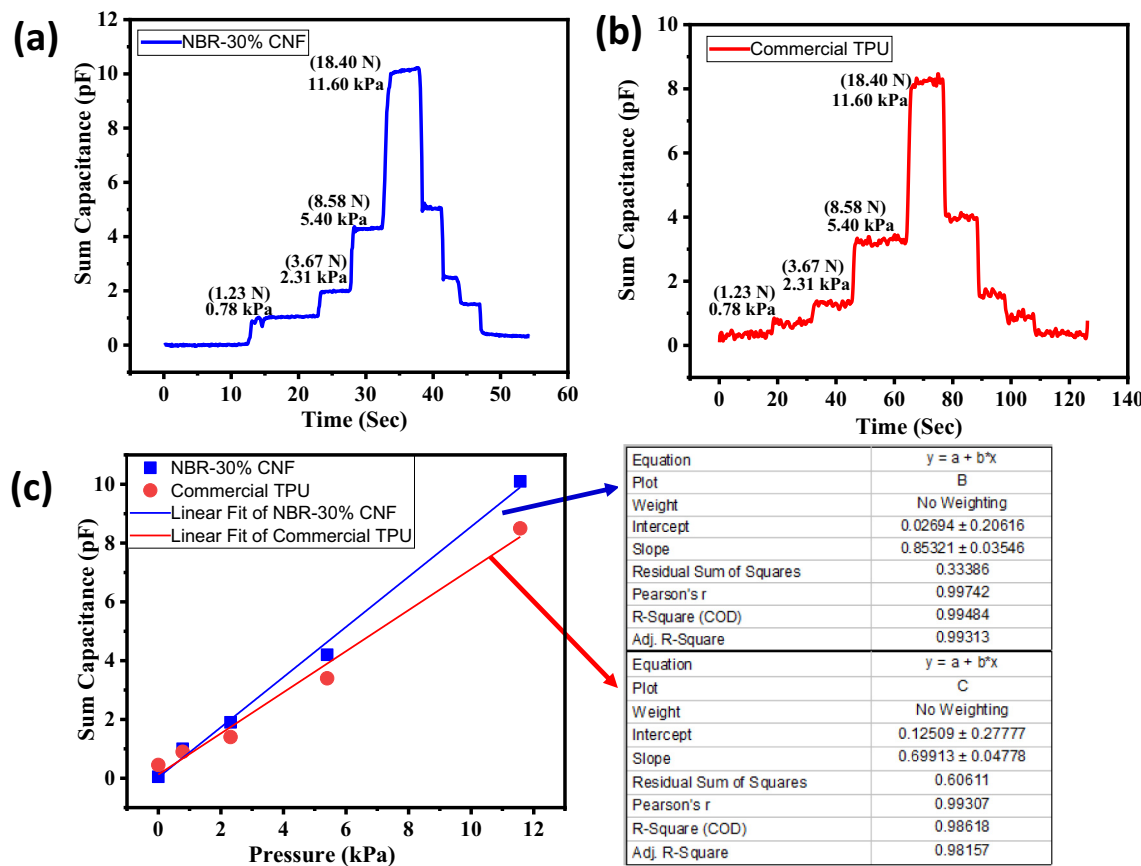


Fig. 9. Capacitive signals from (a) the CNF on nitrile device (b) the commercial copper on TPU device, with increasing loads from 0 to 18.4 N (corresponding to 0–11.6 kPa pressure range) over the deformable mesh, (c) response of the taxels from the devices under test: CNF on nitrile, and commercial Copper on TPU & fit parameters for both samples, top is the CNF device (indicated with blue arrow) and bottom is the copper on TPU device (red arrow). (For interpretation of the references to colour in this figure legend, the reader is referred to the web version of this article.)

Table 2

Comparison between commercial device and nano-ink based one; the parameters useful for tactile sensitivity assessment are reported for both.

Device	NBR-30% CNF	Commercial TPU
Slope (pF/kPa)	0.85 ± 0.03	0.70 ± 0.05
Noise (pF)	0.02	0.08
Minimum detectable pressure (kPa)	0.09	0.22

tronics, even at stretch factors far larger than the ones experienced in joints.

Conclusions

Conducting stretchable coatings based on GNP or CNFs were fabricated with a simple spray coating of conductive suspensions in liquid NR over nitrile rubber films. The sheet resistance of the as-prepared GNP and CNFs coatings was found to be $600 \Omega \text{ sq}^{-1}$ and $30 \Omega \text{ sq}^{-1}$, respectively. Both coatings had excellent adhesion to the nitrile rubber surface and sustained fatigue due to repeated and cyclic elongation tests representing the movement of humanoid robot joints (5%–50% stretching). GNP-based coatings were more sensitive to elongation, which was translated in decreased electrical performance in comparison to CNF-based coatings, even at small elongation levels (5%). For instance, for GNP-based coatings, almost a 100% drop in the initial current was recorded whereas for CNF-based coatings the drop was limited to 50% upon 50% stretching. For this reason, CNF-based coatings were chosen as electrodes for the development of capacitive tactile sensors. Com-

pared to commercial metal electrode printed stretchable tactile systems that can only resist 5% stretching, the present nano-carbon devices can easily adapt to 10 times more stretching levels suitable for extreme robotic motion applications.

Declaration of Competing Interest

The authors declare that they have no known competing financial interests or personal relationships that could have appeared to influence the work reported in this paper.

Appendix A. Supplementary data

Supplementary data to this article can be found online at <https://doi.org/10.1016/j.jiec.2021.05.048>.

References

- [1] A.O. Andrade, A.A. Pereira, S. Walter, R. Almeida, R. Loureiro, D. Compagna, P.J. Kyberd, Biomed. Signal Process Control 10 (2014) 65–78, <https://doi.org/10.1016/j.bspc.2013.12.009>.
- [2] C. Breazeal, 2011 Annual International Conference of the IEEE Engineering in Medicine and Biology Society, IEEE, 2011, pp. 5368–71.
- [3] T. Dahl, M. Boulos, Robotics 3 (1) (2013) 1–21, <https://doi.org/10.3390/robotics3010001>.
- [4] P. Dario, E. Guglielmelli, C. Laschi, G. Teti, Technol. Disabil. 10 (2) (1999) 77–93, <https://doi.org/10.3233/TAD-1999-10202>.
- [5] L. Cai, L. Song, P. Luan, Q. Zhang, N. Zhang, Q. Gao, D. Zhao, X. Zhang, M. Tu, F. Yang, W. Zhou, Q. Fan, J. Luo, W. Zhou, P.M. Ajayan, S. Xie, Sci. Rep. 3 (1) (2013) 3048, <https://doi.org/10.1038/srep03048>.

- [6] T. Yamada, Y. Hayamizu, Y. Yamamoto, Y. Yomogida, A. Izadi-Najafabadi, D.N. Futaba, K. Hata, *Nat. Nanotechnol.* 6 (5) (2011) 296–301, <https://doi.org/10.1038/nnano.2011.36>.
- [7] S.J. Benight, C. Wang, J.B.H. Tok, Z. Bao, *Prog. Polym. Sci.* (2013), <https://doi.org/10.1016/j.progpolymsci.2013.08.001>.
- [8] S. Bauer, S. Bauer-Gogonea, I. Graz, M. Kaltenbrunner, C. Keplinger, R. Schwödauer, *Adv. Mater.* 26 (1) (2014) 149–162, <https://doi.org/10.1002/adma.201303349>.
- [9] C. Pang, G.-Y. Lee, T. Kim, S.M. Kim, H.N. Kim, S.-H. Ahn, K.-Y. Suh, *Nat. Mater.* 11 (9) (2012) 795–801, <https://doi.org/10.1038/nmat3380>.
- [10] A. Schmitz, M. Maggiali, L. Natale, B. Bonino, G. Metta, *IEEE/RSJ 2010 International Conference on Intelligent Robots and Systems, IROS 2010 - Conference Proceedings*, 2010, p. .
- [11] R.S. Dahiya, L. Lorenzelli, G. Metta, M. Valle, *ISCAS 2010 - 2010 IEEE International Symposium on Circuits and Systems: Nano-Bio Circuit Fabrics and Systems*, 2010, p. .
- [12] M. Ramuz, B.C.K. Tee, J.B.H. Tok, Z. Bao, *Adv. Mater.* (2012), <https://doi.org/10.1002/adma.201200523>.
- [13] S. Park, M. Vosguerichian, Z. Bao, *Nanoscale* 5 (5) (2013) 1727, <https://doi.org/10.1039/c3nr33560g>.
- [14] N. Zhang, P. Luan, W. Zhou, Q. Zhang, L. Cai, X. Zhang, W. Zhou, Q. Fan, F. Yang, D. Zhao, Y. Wang, S. Xie, *Nano Res.* 7 (11) (2014) 1680–1690, <https://doi.org/10.1007/s12274-014-0528-6>.
- [15] J.A. Rogers, T. Someya, Y. Huang, *Science* (80-) (2010), <https://doi.org/10.1126/science.1182383>.
- [16] J. Ulmen, M. Cutkosky, *2010 IEEE International Conference on Robotics and Automation, IEEE*, 2010, pp. 4836–41.
- [17] D.S. Patil, S.A. Pawar, J.C. Shin, *J. Ind. Eng. Chem.* 62 (2018) 166–175, <https://doi.org/10.1016/j.jiec.2017.12.054>.
- [18] Y. Wang, Y. Wang, B. Wan, B. Han, G. Cai, R. Chang, *Compos. Part A Appl. Sci. Manuf.* (2018), <https://doi.org/10.1016/j.compositesa.2018.07.017>.
- [19] H. Raghubanshi, E.D. Dikio, E.B. Naidoo, *J. Ind. Eng. Chem.* 44 (2016) 23–42, <https://doi.org/10.1016/j.jiec.2016.08.023>.
- [20] M.D. Dickey, *Adv. Mater.* 29 (27) (2017) 1606425, <https://doi.org/10.1002/adma.201606425>.
- [21] J. Zhou, H. Yu, X. Xu, F. Han, G. Lubineau, *ACS Appl. Mater. Interfaces* 9 (5) (2017) 4835–4842, <https://doi.org/10.1021/acsmami.6b15195>.
- [22] L. Sheng, S. Teo, J. Liu, *J. Med. Biol. Eng.* (2016), <https://doi.org/10.1007/s40846-016-0129-9>.
- [23] Kenry, J.C. Yeo, C.T. Lim, *Microsystems Nanoeng.* (2016), <https://doi.org/10.1038/micronano.2016.43>.
- [24] S. Yaragalla, R. Mishra, S. Thomas, N. Kalarikkal, H.J. Maria, *Carbon-Based Nanofillers and Their Rubber Nanocomposites*, Elsevier, 2019.
- [25] J.R. Potts, D.R. Dreyer, C.W. Bielawski, R.S. Ruoff, *Polymer (Guildf.)* 52 (1) (2011) 5–25, <https://doi.org/10.1016/j.polymer.2010.11.042>.
- [26] S. Yaragalla, R. Rajendran, M.A. AlMaadeed, N. Kalarikkal, S. Thomas, *Mater. Sci. Eng. C* (2019), <https://doi.org/10.1016/j.msec.2019.04.061>.
- [27] B.S. Singu, U. Male, P. Srinivasan, K.R. Yoon, *J. Ind. Eng. Chem.* 49 (2017) 82–87, <https://doi.org/10.1016/j.jiec.2017.01.010>.
- [28] X. Yan, Z. Tai, J. Chen, Q. Xue, *Nanoscale* 3 (1) (2011) 212–216, <https://doi.org/10.1039/CONR00470G>.
- [29] J.E. Mates, I.S. Bayer, J.M. Palumbo, P.J. Carroll, C.M. Megaridis, *Nat. Commun.* (2015), <https://doi.org/10.1038/ncomms9874>.
- [30] X. Wang, S. Meng, M. Tebyetekerwa, Y. Li, J. Pionteck, B. Sun, Z. Qin, M. Zhu, *Compos. Part A Appl. Sci. Manuf.* 105 (2018) 291–299, <https://doi.org/10.1016/j.compositesa.2017.11.027>.
- [31] N.P.S. Chauhan, M. Mozafari, N.S. Chundawat, K. Meghwali, R. Ameta, S.C. Ameta, *J. Ind. Eng. Chem.* 36 (2016) 13–29, <https://doi.org/10.1016/j.jiec.2016.03.003>.
- [32] P. Cataldi, I.S. Bayer, F. Bonaccorso, V. Pellegrini, A. Athanassiou, R. Cingolani, *Adv. Electron. Mater.* 1 (12) (2015) 1500224, <https://doi.org/10.1002/aelm.201500224>.
- [33] <https://www.analog.com/en/products/ad7147.html#product-overview>.
- [34] V. Tikhonoff, A. Cangelosi, P. Fitzpatrick, G. Metta, L. Natale, F. Nori, *Proceedings of the 8th Workshop on Performance Metrics for Intelligent Systems – PerMIS '08, ACM Press, New York, New York, USA, 2008*, p. 57.
- [35] S. Mondal, D. Khastgir, *Compos. Part A Appl. Sci. Manuf.* (2017), <https://doi.org/10.1016/j.compositesa.2017.08.003>.
- [36] L. Valentini, J. Biagiotti, J.M. Kenny, M.A. López Manchado, *J. Appl. Polym. Sci.* 89(10) (2003) 2657–63. 10.1002/app.12319.
- [37] S. Li, Z. Li, T.L. Burnett, T.J.A. Slater, T. Hashimoto, R.J. Young, *J. Mater. Sci.* (2017), <https://doi.org/10.1007/s10853-017-1144-0>.
- [38] B. Likozar, Z. Major, *Appl. Surf. Sci.* (2010), <https://doi.org/10.1016/j.apsusc.2010.07.034>.
- [39] [39] https://www.tss.trelleborg.com/-/media/tss-media-repository/tss_website/pdf-and-other-literature/brochures/mat_chem_comp_gb_en.pdf.
- [40] W. Rong, K.Y. Tong, X.L. Hu, S.K. Ho, *Disabil. Rehabil. Assist. Technol.* 10 (2) (2015) 149–159, <https://doi.org/10.3109/17483107.2013.873491>.
- [41] A.N. Gent, S. Kawahara, J. Zhao, *Rubber Chem. Technol.* (1998), <https://doi.org/10.5254/1.3538496>.
- [42] P. Cataldi, L. Ceseracciu, S. Marras, A. Athanassiou, I.S. Bayer, *Appl. Phys. Lett.* 110 (12) (2017), <https://doi.org/10.1063/1.4978865>.
- [43] P. Cataldi, I.S. Bayer, G. Nanni, A. Athanassiou, F. Bonaccorso, V. Pellegrini, A.E. del Rio Castillo, F. Ricciardella, S. Artyukhin, M.A. Tronche, Y. Gogotsi, R. Cingolani, *Carbon N. Y.* 109 (2016) 331–9. 10.1016/j.carbon.2016.08.026.
- [44] C.S. Lim, A.J. Rodriguez, M.E. Guzman, J.D. Schaefer, B. Minaie, *Carbon N. Y.* (2011), <https://doi.org/10.1016/j.carbon.2011.01.010>.
- [45] A. Schmitz, P. Maiolino, M. Maggiali, L. Natale, G. Cannata, G. Metta, *IEEE Trans. Robot.* 27 (3) (2011) 389–400, <https://doi.org/10.1109/TRO.2011.2132930>.
- [46] P. Maiolino, M. Maggiali, G. Cannata, G. Metta, L. Natale, *IEEE Sens. J.* 13 (10) (2013) 3910–3917, <https://doi.org/10.1109/JSEN.2013.2258149>.
- [47] <https://fineline-global.com/en/knowledge-scb>.
- [48] <https://esd.eu/en/products/can-usb2>.